Space Vectors and Pseudo Inverse Matrix Methods for the Radial Force Control in Bearingless Multi-Sector Permanent Magnet Machines

G. Sala, G. Valente, A. Formentini, L. Papini, D. Gerada, P. Zanchetta, A. Tani, C. Gerada,

***Abstract*—Two different approaches to characterize the torque and radial force production in a Bearingless Multi-Sector Permanent Magnet (BMSPM) machine are presented in this work. The first method consists of modelling the motor in terms of torque and force production as a function of the stationary reference frame $\alpha - \beta$ currents. The current control reference signals are then evaluated adopting the Joule losses minimization as constrain by means of the pseudo inverse matrix. The second method is based on the control of the magnetic field harmonics in the airgap through the current Space Vector (SV) technique. Once the magnetic field harmonics involved in the torque and force production are determined, the SV transformation can be defined to obtain the reference current space vectors.**
The methods are validated by numerical simulations, Finite Element Analysis (FEA) and experimental tests. The differences in terms of two Degrees of Freedom (DOF) levitation performance and efficiency are highlighted in order to give the reader an in-depth comparison of the two methods.

***Index Terms*—Analytical models, Displacement control, Force control, Machine vector control, Magnetic levitation, Permanent Magnet machines.**

I. Introduction

The bearing element is one of the most critical component when dealing with high rotational speed and reliability of electrical machines [1]. The magnetic levitation would allow to overcome the aforementioned issues as well as to eliminate the bearing friction, the maintenance and the monitoring [2]. Nowadays, Active Magnetic Bearings (AMB) are the most exploited technology for the levitation. They are employed in several industrial and commercial applications such as compressors, spindles, flywheels and generators where high rotation speed is a requirement [3]–[5]. However, magnetic bearings generally lead to an increased overall length of the machine, added weight and higher cost of the drive. To this regard, Bearingless Motors (BMs) offer the advantage to generate both torque and suspension force in a single machine structure, consequently maximizing the power to weight and power to volume ratio. The most exploited method to produce a controllable suspension force consists of providing the BMs with two separate windings, one responsible for motoring (torque generation) and the other for levitation (force generation). Several papers can be found in the literature adopting the two-winding configuration for bearingless operation [6]–[8]. However, the additional winding is still not a completely embedded solution. Therefore, more recently different solutions have been proposed, among which the multi-phase BM is one of the most promising since it presents simpler construction, higher power density and better fault tolerance capabilities [9]–[12].

Considerable efforts have been made to exploit the multi-phase technology in different fields such as sensorless drives [13], on-line diagnosis algorithms [14], [15] and fault tolerant controls [16], [17]. The development of multiphase machines suitable for the radial force control is another example of this technology advancement. The multi-sector winding design of a permanent magnet machine, where independent three-phase windings are located in different stator areas (sectors), is a possible multiphase solution to allow a radial force control. The complexity of the control of such a system emerges when a detailed analysis is carried out to allow a radial force control, as in this work, or if asymmetries and faults are taken into account in order to avoid performance deterioration [18]–[21].

The main objective of this paper is the validation of two different radial force and torque control techniques applied to a MSPM machine. The first one exploits the Moore-Penrose pseudo inverse of the machine model matrix formulation to obtain those $\alpha - \beta$ reference currents that generate the required force and torque minimizing the Joule losses [22], [23]. Instead, the second method exploits the SV technique to generate appropriate magnetic field harmonics in the airgap responsible for both torque and radial force generation [18], [19]. Both the methods are employed to achieve a two DOF bearingless operation.

To start with, a brief theoretical introduction of the two techniques is provided. Both numerical and FE simulation results are used to compare the two methods in terms of efficiency and force control performance. Finally, experimental tests are performed to validate the proposed techniques for the prototype machine, consisting of a conventional 18 slot - 6 poles PMSM with a re-arranged winding configuration.

Manuscript received September, 2017; revised December, 2017; accepted January, 2018. A. Tani is with the Department of Electrical and Electrical Engineering, University of Bologna, Bologna. G. Sala, G. Valente, A. Formentini, L. Papini, D. Gerada, P. Zanchetta and C. Gerada are with the PEMC group, University of Nottingham, Nottingham, NG7 2RD, UK (e-mail: giacomo.sala2@nottingham.ac.uk).

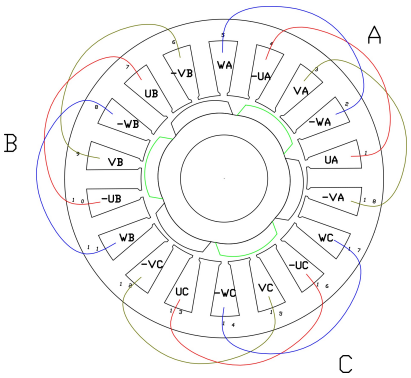

Fig. 1. Cross section of the 18 slots - 6 poles 3 sectors PM machine.

II. Radial Force Production for Multi-Sector Permanent Magnet Machines

A. MSPM machine winding

The cross section of the MSPM machine considered in this work is shown in Fig. 1. Three three-phase full-pitched distributed windings with independent star connections are located 120 deg apart in three stator sectors ($n_s = 3$). The main machine design parameters are listed in Table I.

TABLE I
Machine Parameters

Parameter	Value
Pole number ($2p$)	6
PM material	NdFeB
Power rating	1.5 [kW]
Rated Speed (ω_m)	3000 [rpm]
Rated torque (T_{rated})	5 [Nm]
Turns/coil (N)	22
Phase resistance (R_{ph})	0.0808 [Ohm]
Line to line voltage constant (k_V)	15.5 [V/krpm]
PM flux of one sector ($^s\Lambda_{PM}$)	0.0284 [Wb]
Torque constant (K_T)	0.434 [Nm/A]
Outer stator radius	47.5 [mm]
Inner stator diameter	24.75 [mm]
Mid-airgap radius (r_g)	24.25 [mm]
Axial length (l_a)	90 [mm]
Airgap length (δ_0)	1 [mm]
Magnets thickness	4 [mm]

B. Theoretical description of the torque and radial force control methods

The spatial harmonic orders of the armature and PM flux density have to be identical in order to produce a net torque in a permanent magnet machine. The main harmonic order is usually the one related to the number of pole pairs (p). On the other hand, the radial force can be produced commanding a flux density of order $p\pm1$. Hence, being $p = 3$ in the analysed machine, the interaction of the 3^{rd} permanent magnet flux density harmonic with the 2^{nd} and 4^{th} armature flux density harmonics causes the radial force. In the next paragraphs the two different torque and force control techniques are presented. Both methods rely on the assumptions of linear materials and radially centred rotor. As a matter of fact, the radial position displacement has been taken into account in [23] introducing the stiffness constant that describes the linear relationship between $x-y$ axis position and force. Only the current contribution to the radial force and torque has been reported in the next paragraphs, while the stiffness term has been used in the synthesis of the PID position regulator.

1) Pseudo Inverse Matrix Method (PIM): The PIM method is based on electromagnetic characterization of the machine in terms of total force (F_x, F_y) and torque (T) as a function of the α-β currents of each s^{th} three-phase winding ($^si_\alpha, ^si_\beta$). The matrix formulation of the $x-y$ force components and torque of the generic sector s can be expressed as follows:

$$^s\bar{W}_E(\vartheta_e, ^s\gamma, ^s\bar{i}_{\alpha\beta}) = {}^s\mathbf{K}_E(\vartheta_e, ^s\gamma)\ ^s\bar{i}_{\alpha\beta} \tag{1}$$

where $\vartheta_e = p\vartheta_m$ (being ϑ_m the mechanical rotor position) is the electrical angular rotor position and $^s\gamma$ is the angular position of the s^{th} winding axis with respect to the $x-$axis, $^s\bar{W}_E = \begin{bmatrix}^sF_x & ^sF_y & ^sT\end{bmatrix}^T$ and $^s\bar{i}_{\alpha\beta} = \begin{bmatrix}^si_\alpha & ^si_\beta\end{bmatrix}^T$. Matrix $^s\mathbf{K}_E \in \mathbb{R}^{3\times2}$ can be expressed as (2).

$$^s\mathbf{K}_E(\vartheta_e, ^s\gamma) = \begin{bmatrix} ^sk_{x,\alpha}(\vartheta_e, ^s\gamma) & ^sk_{x,\beta}(\vartheta_e, ^s\gamma) \\ ^sk_{y,\alpha}(\vartheta_e, ^s\gamma) & ^sk_{y,\beta}(\vartheta_e, ^s\gamma) \\ ^sk_{T,\alpha}(\vartheta_e) & ^sk_{T,\beta}(\vartheta_e) \end{bmatrix} \tag{2}$$

In [22] and [23] the coefficients of the above matrix formulation are calculated for each machine sector. In particular, in [23] the rotor radial position has been taken into account in the coefficients expressions showing that, within the maximum displacement considered, the maximum variation is less than 9%. Therefore, matrix $^s\mathbf{K}_E(\vartheta_e, ^s\gamma)$ is assumed radial position independent in this paper.
The total force and torque are evaluated by summing the contributions of the three sector windings defined by (1) as follows:

$$\bar{W}_E(\vartheta_e, \bar{\gamma}, \bar{i}_{\alpha\beta}) = \begin{bmatrix} ^AF_x + {}^BF_x + {}^CF_x \\ ^AF_y + {}^BF_y + {}^CF_y \\ ^AT + {}^BT + {}^CT \end{bmatrix} = \mathbf{K}_E(\vartheta_e, \bar{\gamma})\bar{i}_{\alpha\beta} \tag{3}$$

where: $\bar{\gamma} = \begin{bmatrix}^A\gamma & ^B\gamma & ^C\gamma\end{bmatrix}$; $\mathbf{K}_E = \begin{bmatrix}^A\mathbf{K}_E & ^B\mathbf{K}_E & ^C\mathbf{K}_E\end{bmatrix}^T$; $\bar{i}_{\alpha\beta} = \begin{bmatrix}^Ai_\alpha & ^Ai_\beta & ^Bi_\alpha & ^Bi_\beta & ^Ci_\alpha & ^Ci_\beta\end{bmatrix}^T$.
The current reference vector $\bar{i}^*_{\alpha\beta}$ can be obtained inverting the matrix $\mathbf{K}_E \in \mathbb{R}^{3\times2n_s}$. However, the latter results in a rectangular matrix since the dimension of $\bar{W}_E$ is smaller than the number of state variables ($3 < 2n_s$), hence the system is under-determined with an infinite number of solutions. The minimization of the Joule losses is chosen as problem constrain leading to the Moore-Penrose pseudo inverse matrix expression [22]:

$$\mathbf{K}^+_E(\vartheta_e, \bar{\gamma}) = \mathbf{K}^T_E(\vartheta_e, \bar{\gamma}) \left[\mathbf{K}_E(\vartheta_e, \bar{\gamma})\, \mathbf{K}^T_E(\vartheta_e, \bar{\gamma})\right]^{-1} \tag{4}$$

The reference current vector needed to produce the desired mechanical output vector $\bar{W}_{E,ref}$ is evaluated by:

$$\bar{i}_{\alpha\beta,ref} = \mathbf{K}^+_E(\vartheta_e, \bar{\gamma})\, \bar{W}_{E,ref} \tag{5}$$

Finally, the coefficients of $\mathbf{K}^+_E$ are approximated with their fundamental harmonic waveform in order to reduce the computational efforts of the control platform [22].

2) Space Vector Method (SV): The SV method considers the machine as an unique device that can be controlled to generate appropriate field harmonics in the airgap [18], [19]. The modelling of the radial force in the SV model is based on the evaluation of the Maxwell stress tensors neglecting the tangential component of the flux density. Indeed, the Maxwell stress tensor $\hat{\sigma}_{r\tau}$ (r and τ indicate the radial and a tangential components) in absence of electric field can be expressed as:

$$\hat{\sigma}_{r\tau} = \sigma_\tau \hat{\tau} + \sigma_r \hat{r} = \frac{B_r B_\tau}{\mu_0}\hat{\tau} + \frac{B_r^2 - B_\tau^2}{2\mu_0}\hat{r} \tag{6}$$

From the radial and tangential components of the stress tensor, the overall radial force acting on the rotor of an electrical machine can be evaluated as:

$$\hat{F} = \int_0^{l_a}\int_0^{2\pi} (j\sigma_\tau(\vartheta_s, z)e^{j\vartheta_s} + \sigma_r(\vartheta_s, z)e^{j\vartheta_s}) r_g d\vartheta_s dz \tag{7}$$

where ϑ_s identifies the angular position in the stator reference frame, r_g is the middle airgap radius, and l_a the machine active length. Substituting the radial and tangential components of the stress tensor (6) in (7), writing the flux distribution in its Fourier series coefficients and considering $B = \mu_0 H$, yields to the following equation:

$$\begin{aligned}\hat{F} = j\frac{\pi\mu_0 r_g l_a}{2}\sum_{\rho=1}^{\infty}(\hat{H}_{r,\rho}\hat{H}^*_{\tau,\rho-1} + \hat{H}_{r,\rho}\hat{H}^*_{\tau,\rho+1}) + \\ + \frac{\pi\mu_0 r_g l_a}{4}\sum_{\rho=1}^{\infty}(\hat{H}_{r,\rho}\hat{H}^*_{r,\rho-1} + \hat{H}_{r,\rho}\hat{H}^*_{r,\rho+1}) + \\ - \frac{\pi\mu_0 r_g l_a}{4}\sum_{\rho=1}^{\infty}(\hat{H}_{\tau,\rho}\hat{H}^*_{\tau,\rho-1} + \hat{H}_{\tau,\rho}\hat{H}^*_{\tau,\rho+1})\end{aligned} \tag{8}$$

where the magnetic field harmonics are related to both the current and the magnet magnetomotive forces.
If the tangential component of the magnetic field in the airgap is neglected ($\hat{H}_{\tau,h} = 0$), the formulation of the torque and radial force (8) as a function of the field harmonics is described by the following approximated relationship:

$$\begin{bmatrix}\hat{F}_{p-1}\\ \hat{F}_{p+1}\\ T\end{bmatrix} = k_c \begin{bmatrix}\hat{H}_{M,p}\hat{H}^*_{C,p-1}e^{-jp\vartheta_m}\\ \hat{H}_{M,p}\hat{H}^*_{C,p+1}e^{jp\vartheta_m}\\ 2\delta\ \Re\{jp\hat{H}_{M,p}\hat{H}^*_{C,p}e^{jp\vartheta_m}\}\end{bmatrix} \tag{9}$$

$$\hat{F} = \hat{F}_{p-1} + \hat{F}_{p+1} \tag{10}$$

where $\hat{F}$ is the resulting force vector ($F_x + jF_y$ or $Fe^{j\vartheta_f}$), while $\hat{F}_{p-1}$ and $\hat{F}_{p+1}$ are the main force contributions, related to the $(p-1)^{th}$ and $(p+1)^{th}$ field harmonics. k_c is equal to $\frac{\pi}{2}\mu_0 r_g l_a$, $\hat{H}_{M,p}$ represents the p^{th} harmonic of permanent magnet field in the rotor reference frame, $\hat{H}_{C,p-1}$, $\hat{H}_{C,p}$ and $\hat{H}_{C,p+1}$ represent the $(p-1)^{th}$, p^{th} and $(p+1)^{th}$ harmonics of the armature field; l_a is the stator active length; r_g is the mid-airgap radius; δ is the airgap thickness including the magnets. The relation between the armature field harmonics and the related currents space vectors, which allows the independent control of the main field harmonics, is [18]:

$$\hat{H}_{C,\rho} = \frac{24N\sin\rho\Delta\varphi}{2\rho\pi\delta}\hat{i}_\rho \tag{11}$$

where N is the number of turns per phase, $\Delta\varphi$ is the coil pitch and $\hat{i}_\rho$ is the ρ-th current space vector defined by the following Clarke transformation, adapted to the analysed machine:

$$\hat{i}_\rho = \frac{2}{9}\underbrace{\sum_{k=18,1,2,6,7,8,12,13,14} i_k e^{j\rho\varphi_k}}_{slots} \tag{12}$$

where k is the number of the slot where each phase appears following the slots clockwise, i_k is the current in the k^{th} slot and φ_k is equal to $\frac{2\pi}{18}(k-1)$.
The expression of the resultant force vector can be written as follows, observing (11) and (12), and considering the pole pairs number of the machine ($p = 3$):

$$\hat{F} = (F_2 + F_4)e^{j\vartheta_f} = K_{F2}\hat{i}^*_2 e^{j3\vartheta_m} + K_{F4}\hat{i}_4 e^{-j3\vartheta_m}. \tag{13}$$

where ϑ_f is the angle of the resulting force vector, $F2$ and $F4$ are the contributions of the 2^{nd} and 4^{th} magnetic field harmonics to the total force production, and the evaluation of the force constants K_{F2} and K_{F4} is presented in [18], [19]. The values of K_{F2} and K_{F4} are 9.60 N/A and 17.85 N/A, respectively. Finally, the current space vectors needed to generate the torque and radial force are defined by

$$\begin{bmatrix}\hat{i}_{2,ref}\\ \hat{i}_{4,ref}\\ \hat{i}_{3,ref}\end{bmatrix} = \begin{bmatrix}(F2_{ref}/K_{F2})e^{j3\vartheta_m - \vartheta_f}\\ (F4_{ref}/K_{F4})e^{j3\vartheta_m + \vartheta_f}\\ j(T_{ref}/K_T)e^{j3\vartheta_m}\end{bmatrix} \tag{14}$$

where K_T is the torque constant. The SV control algorithm is based on the three vectorial equations in (14), the first two are responsible for the force generation and the third one describes completely the torque production. Because the 2^{nd} and 4^{th} current space vectors can be controlled independently by the 3^{rd} one, the control of the force by the SV method is completely independent from the torque one [18], [19]. Furthermore, each current space vector can be controlled in a reference frame synchronous with the reference vector as:

$$\begin{bmatrix}\hat{i}_{2,syn,ref}\\ \hat{i}_{4,syn,ref}\\ \hat{i}_{3,syn,ref}\end{bmatrix} = \begin{bmatrix}(F2_{pu})F_{ref}/K_{F2}\\ (1 - F2_{pu})F_{ref}/K_{F4}\\ jT_{ref}/K_T\end{bmatrix} \tag{15}$$

where $F2_{pu}$ is the force, in per unit, produced by the 2^{nd} order harmonic of the armature field. In other words, this new quantity is the ratio between the contribution of 2^{nd} magnetic field harmonic to the force and the force magnitude. This parameter has been introduced as a further degree of freedom in the control, and its effects on the machine performance are analysed in the following sections.
It is worth noticing that the assumption of neglecting the magnetic field tangential component in the SV model leads to imprecise values of the force constants (K_{F2} and K_{F4}). Therefore, the latter should be matched with FEA in order to take into account for the effect of the tangential component, and all the field harmonic interactions in (8).

C. Bearingless operation

The block diagram of the BMSPM motor control scheme is shown in Fig. 2. The two torque and radial force control

techniques are highlighted using different colours: the PIM control on the top (green) and the SV control on the bottom (red). With "INV Clarke" are named the inverse Clarke transformations needed by the two control algorithms.
The speed control relies on a standard PI regulator. The output of the speed controller is the reference torque, used as input of the PIM and SV blocks. The radial rotor position is measured by two displacement sensors positioned along the $x-$ and $y-$ axis. The measured radial position is compared with its reference value and the displacement errors are used as the inputs of two ($x-$ and $y-$ axis) PID regulators in order to determine the reference force.

1) PIM technique: The PIM control technique defines, by means of (5), the $\alpha-\beta$ reference currents for each motor sector once the torque and radial force references are defined. However, for the purpose of the current control, each $\alpha-\beta$ reference current vector is transformed in the $d-q$ axis reference frame by a standard Park transformation in order to allow a Field Oriented Control (FOC) for the torque. Standard PI regulators are used to define the reference voltages in the $d-q$ reference frame and the back-EMF is compensated in feed-forward before the Park and Clarke inverse transformations are applied, as in a three-phase PM machine control. Finally, the three-phase reference voltages are modulated by a traditional PWM technique in order to define the gate driver signals for the control of each inverter.

2) SV technique: The SV control technique exploits the multi-sector current space vectors to produce the torque and force related armature field harmonics. Observing (9) it is straightforward to notice that, in the machine under investigation, only the 3^{rd} harmonic is related to the torque production while both the 2^{nd} and the 4^{th} contribute to the force generation. Therefore, the contribution of the two harmonics to the force in per unit ($F2_{pu}$ and $F4_{pu} = 1 - F2_{pu}$ respectively) can be used as a degree of freedom to optimize the control technique. The machine multi-sector current space vectors are defined in the reference frames synchronous with the related field harmonics using (15). This allows obtaining only non zero $d2-$ and $d4-$axis reference current components for the force production and $q3-$axis reference current component for the torque production in every working condition.
Furthermore, the back-EMF has to be compensated only for the 3^{rd} voltage space vector since the permanent magnets do not generate the 2^{nd} and 4^{th} field harmonics in the airgap if the eccentricity is neglected. Hence a wrong back-EMF evaluation affects only the torque control.
Finally, the synchronous voltage space vectors are rotated to the stationary reference frame by three different Park transformations, and the phase reference voltages required for the inverter control are defined using the generalized inverse Clarke transform for multi-sector machines, as in [18], [19].

III. Numerical Simulations

The machine control has been verified by simulations in Matlab-Simulink environment. The machine model is derived by means of multi-static non-linear FE simulations in MagNet. The FE model is the one shown in Fig. 1 and the main parameters are listed in Table I. For each static simulation the rotor is rotated by a small angle ($\Delta\vartheta$) and each sector is fed with current values ranging from $-i_{rated} \div i_{rated}$ (with 1 A steps). The obtained $x-y$ force components and torque are stored in the form of lookup table in the Simulink model and a linear method has been used to interpolate the lookup table elements.
The simulation results shown in Fig. 3 present a force reference rotating at the same frequency of the rotor and with magnitude proportional to the square value of the rotating speed is commanded in open loop. A rotating reference force can represent for instance, the force required to compensate an unbalance in the rotor mass once the related dynamic

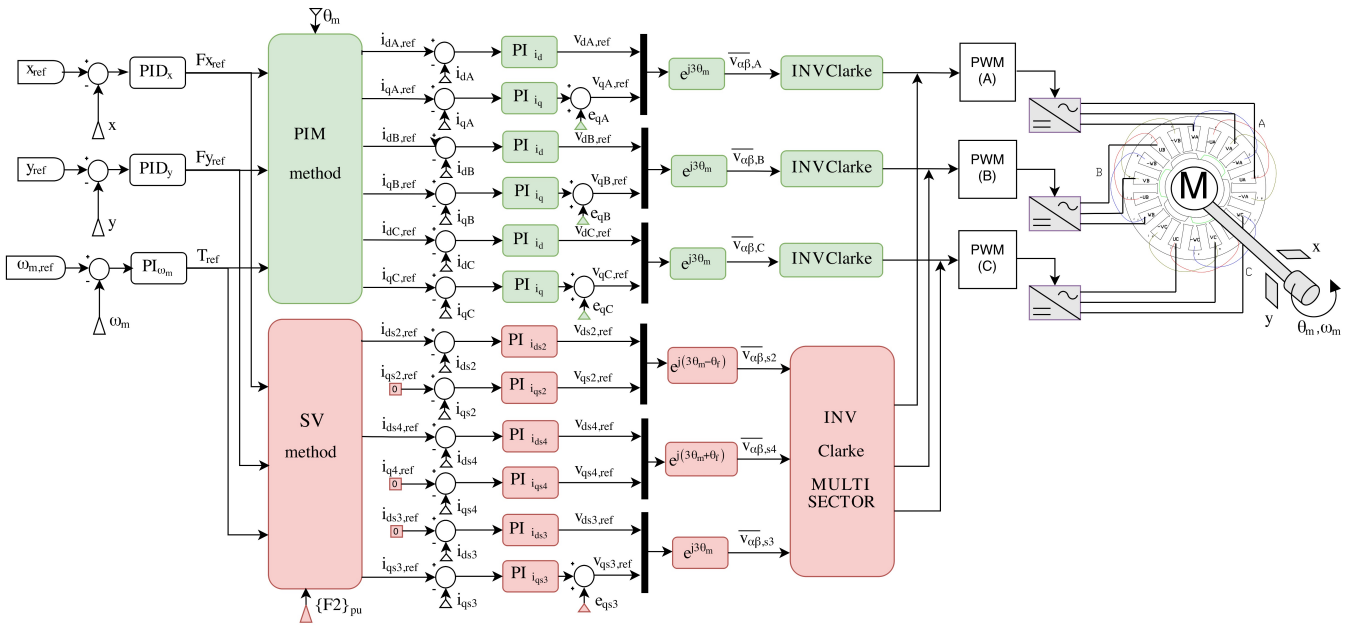

Fig. 2. Comparison of the two control schemes: the PIM control on the top (green) and the SV control on the bottom (red).

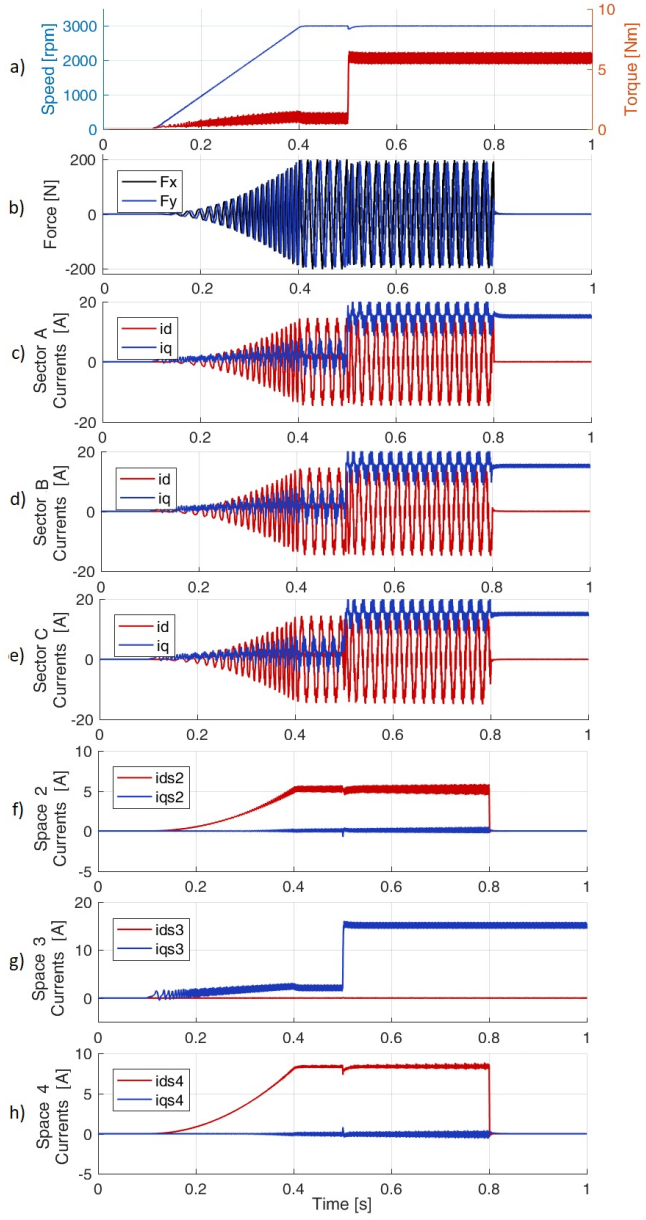

Fig. 3. Numerical simulation results of a speed transient at no load from 0 to 3000 rpm, followed by a torque step of 5 Nm (at 0.5 s). The radial force is synchronous with the rotor as in a static unbalance in the rotor mass till 0.8 s, when the force is set to zero again. The speed, torque (a) and force (b), the dq currents of each sector (c-e) and the dq current space vector components (f-h) are plotted.

behaviour is known [24]. At first, a speed ramp from 0 to 3000 rpm (rated speed) has been applied. At 0.5 s a load equal to the rated torque T_{rated} is applied. The reference force is finally set to zero at 0.8 s. The simulation has been reported only for the SV control with the $F2_{pu}$ value chosen as for the PIM method (this assumption is clarified in the next Section), because, owing to the high dynamic of the control system, the performances of the two control techniques do not show significant differences in the numerical simulations. Instead, the measured currents of the simulation (inputs to the PI regulators) are reported for both the methods as in the scheme of Fig. 2. Comparing Fig. 3c-3e with Fig. 3f-3h, it can be observed that the reference current space vector components have significantly different waveforms in the two methods. As a matter of fact, the PIM method produces sinusoidal $d-q$ reference currents (Fig. 3c-3e) when a sinusoidal force is commanded. It can be notice that both $d-$ and $q-$axis currents take part in the force production, while only DC $q-$axis currents are needed to produce torque. On the other hand, the current references generated by the SV method are constant in steady state operation, as highlighted by (15). The above observation allows identifying an important difference in the two methods under examination. In particular, it is well known that the performance of a PI regulator deteriorates when a sinusoidal input is applied; hence, the SV method allows better control performance in case of synchronous force control.

IV. Finite Element Simulations

Transient FE simulations have been performed in order to validate the predicted performance in the computational environment (MagNet). The machine losses and efficiency are evaluated using the SV method for different values of the force produced by the 2^{nd} order harmonic of the armature field in per unit ($F2_{pu}$) in order to define which is the value that optimizes the machine performance. A view of the flux and the current density in the slots is shown in Fig. 4 for different $F2_{pu}$ values, spinning the rotor at 3000 rpm and commanding 200 N force on the $y-$ axis and 5 Nm torque. 200 N is around the rated force of the machine when the torque is zero, and it is more that 10 times the rotor weight force. Also the results for rated torque operating condition and no force control are shown. It can be observed that having $F2_{pu}$ equal to 0.25 and 0.5 results in more uniform current density and flux density distribution.

1) Joule Losses: Fig. 5 shows the analytical and FE evaluation of the stator copper Joule losses at rated torque and 3000 rpm as function of the $F2_{pu}$ parameter.

The minimum Joule losses are reached for about $F2_{pu} = 0.25$. This result is the same founded by the PIM method. Because of the importance of this value of $F2_{pu}$, a simplified evaluation of the levitating performance (with a 20 N of reference force, that is almost the rotor weight) is shown, highlighted with an asterisk, for $F2_{pu} = 0.25$. It is worth noticing that a non optimized choice of $F2_{pu}$ also results in a non homogeneous copper losses distribution among the sector windings, with localized hot spots in the more stressed sector. The Joule losses distribution among the sectors is shown in Fig. 6. The Joule losses as function of the $F2_{pu}$ value and for a given torque and force are evaluated by the following equation:

$$P_J = R_{ph}[(J_{F,2}F2_{pu}^2 + J_{F,1}F2_{pu} + J_{F,0})F^2 + J_T T^2] \quad (16)$$

where the related losses parameters are presented in Table III. The demonstration of (16) is presented in the Appendix. As expected, the analytical losses evaluation gives the same result of the FEA (Fig. 5).

2) Iron Losses and Efficiency: The PIM control algorithm is based on the copper Joule losses minimization. However, even if the PIM method already optimizes the $F2_{pu}$ value in

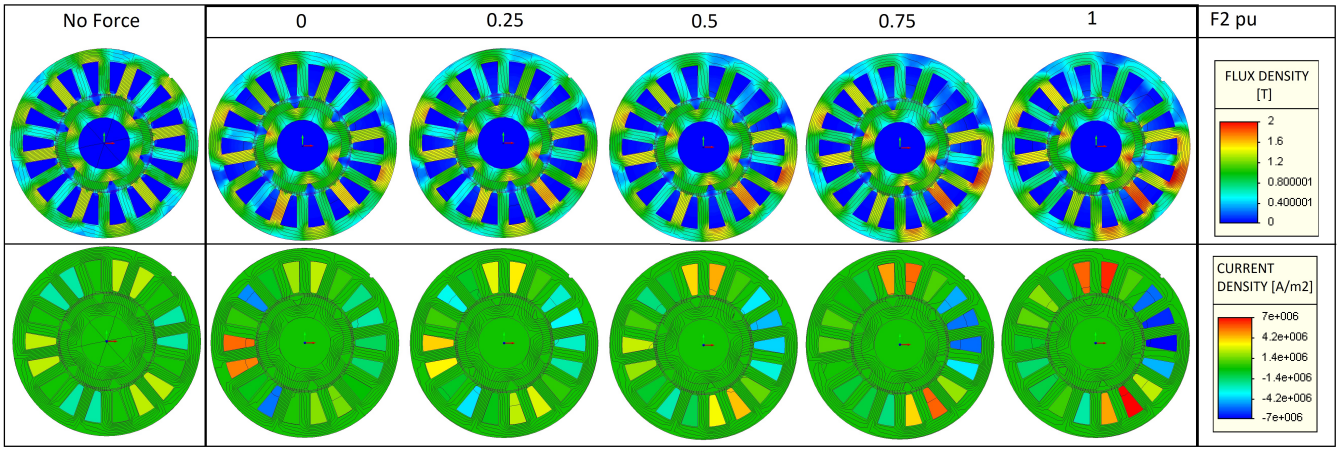

Fig. 4. Views of the flux density and the slots current density at rated torque. On the left there is a view of the machine working without force control. On the other views the reference force is 200 N and $F2_{pu}$ is varied from 0 to 1.

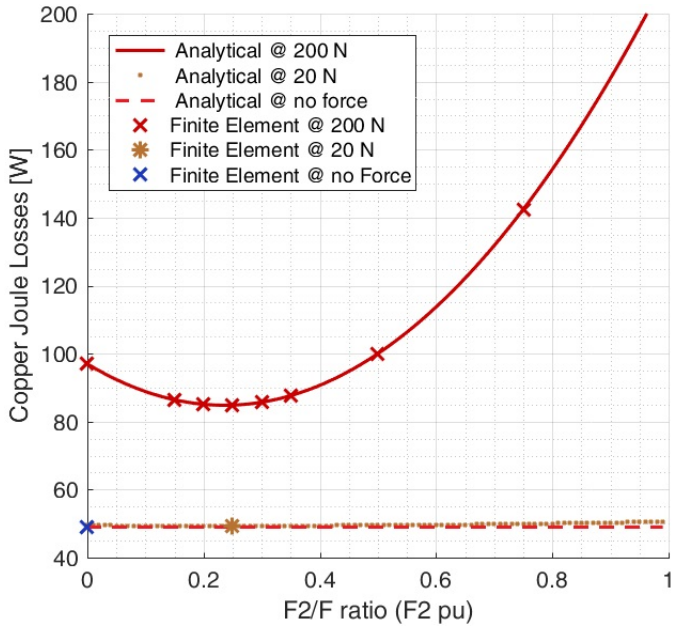

Fig. 5. Analytical and FEA evaluation of the machine Joule losses at rated torque varying $F2_{pu}$.

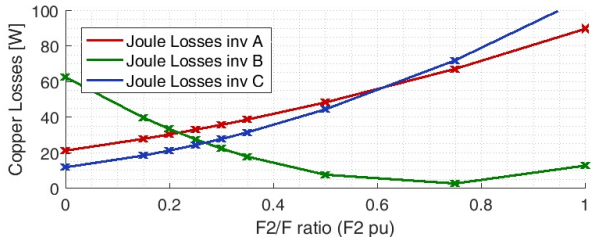

Fig. 6. Machine copper Joule losses related to the three sector windings, at rated torque and 200 N force on the y-axis varying $F2_{pu}$. FEA results.

order to minimize the copper Joule losses, it does not take into account the iron losses (hysteresis and eddy). However, the minimum of the iron losses remains the same as the one that minimizes the Joule losses ($F2_{pu} = 0.25$). Furthermore, because the flux in a SPM machine is mainly produced by the magnets, the iron losses do not change as much as the copper

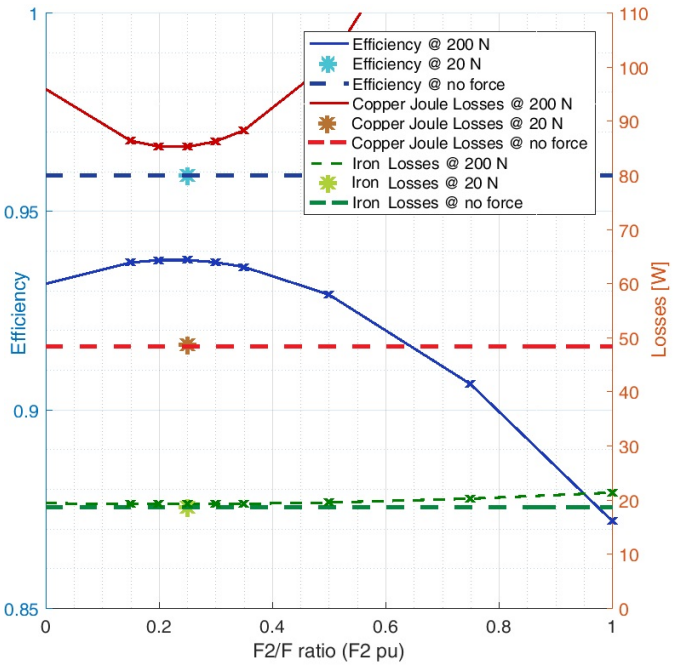

Fig. 7. Machine efficiency and losses varying $F2_{pu}$. FEA results.

ones when the phase currents are increased for the radial force control. The iron losses and the efficiency of the machine are summarized in Fig. 7 with and without radial force control, neglecting the extra-losses (as friction and ventilation related ones) considering that the levitation final goal is also to significantly reduce them.

It is worth noticing that the electrical efficiency drop related to the force control is negligible for the considered case study. Indeed, in case of a force load of about 10 times the rotor weight the efficiency decreases of about 2.2 % (from 95.91 to 93.79). This result can be considered as a benchmark to compare the proposed solution with alternative levitation systems.

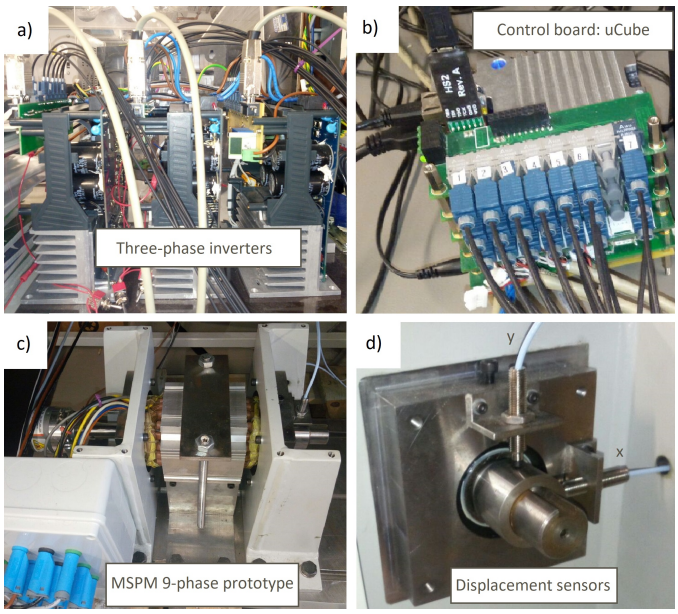

Fig. 8. a) The three three-phase inverters. b) The control board. c) the machine prototype and test rig. d) the rotor shaft with the displacement sensors.

V. Experimental Validation

A. Description of the Experimental set-up

Fig. 8 details the experimental set-up in all its parts.

Fig. 8a shows the three three-phase inverters, each of them connected to one of the MSPM motor winding (Fig. 8c). The inverters, equipped with a standard IGBT power module with switching frequency $F_s = 10$ kHz, are independently controlled by means of a centralized control platform [25] (Fig. 8b) that communicates with the power modules gate drives by means of fibre optic cables. In order to realize a bearingless drive with two mechanical degrees of freedom, the tilting movement and the axial displacement is constrained by a self-alignment bearing mounted on one side of the shaft. The other side is free to only move along the $x-y$ axes within a certain displacement, given by the clearance of the backup bearing (150 μm). Fig. 8d shows the two displacement probes mounted on the backup bearing housing along the $x-y$ axes.

B. Comparison of the PIM and SV methods

The experimental tests have been performed to validate and compare the two control techniques for a two degrees of freedom bearingless operation. The tuning of the radial position and speed regulators is kept identical while testing the PIM and SV methods.

1) Open loop rotating force: A rotating reference force is applied in open loop in order to experimentally verify the numerical simulation results obtained in Section III. Therefore, the aim of the test is to confirm the difference in the currents generated by the PIM and SV methods. The experimental results are shown in Fig. 9. The maximum operating speed is limited to 600 rpm because the test is performed without the position control and the shaft position is constrained only by the backup bearing. The frequency of the rotating force is equal to the rotor mechanical frequency while the magnitude increases with the square of the speed, commanding 200 N at 600 rpm. In Fig. 9 it is possible to observe that the $d-q$ axes currents of the three sectors generated by the PIM method (Fig. 9c-9e) are sinusoidal, while the SV current space vector components (Fig. 9f-9h) are constant. This is in accordance to the result obtained by the numerical simulation in Section III.

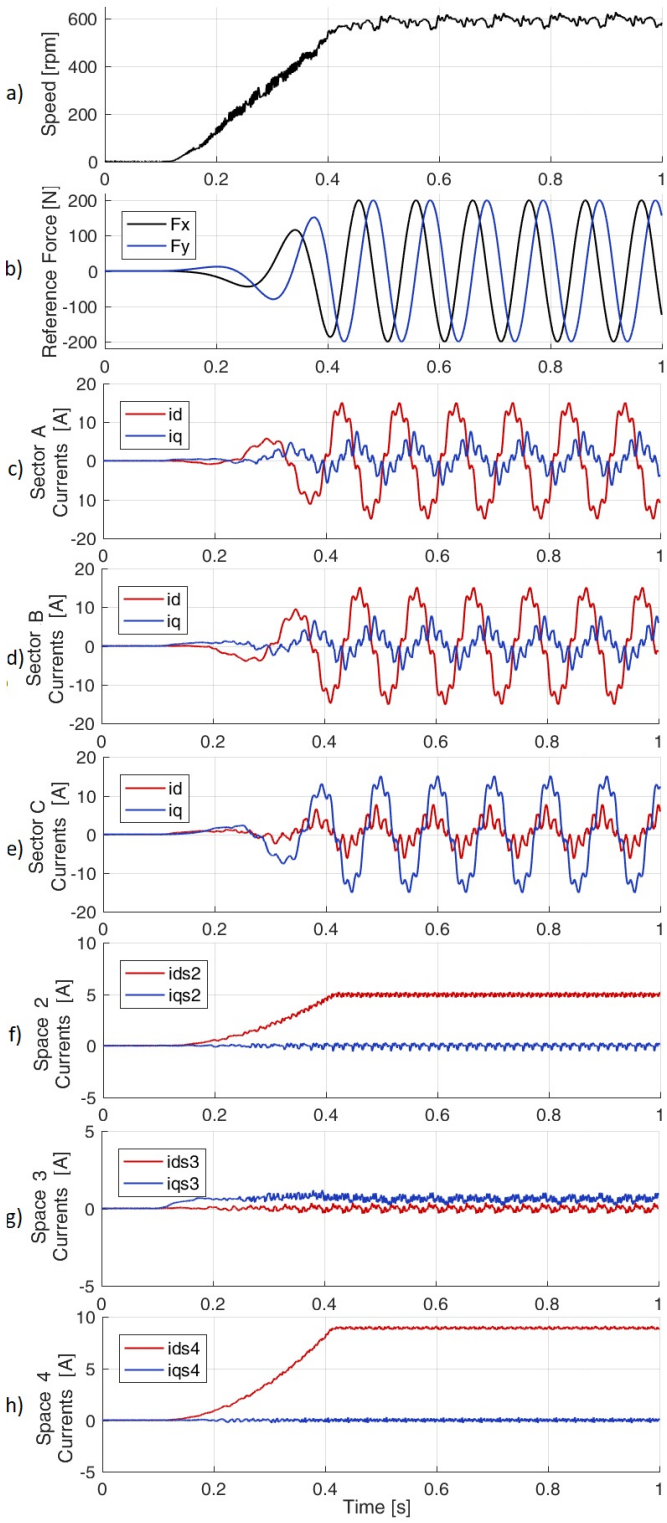

Fig. 9. Experimental results of a speed transient at no load from 0 to 600 rpm. The radial force is synchronous with the rotor as in a static unbalance in the rotor mass. The speed (a) and force (b), the dq currents of each sector (c-e) and the dq current space vector components (f-h) are plotted.

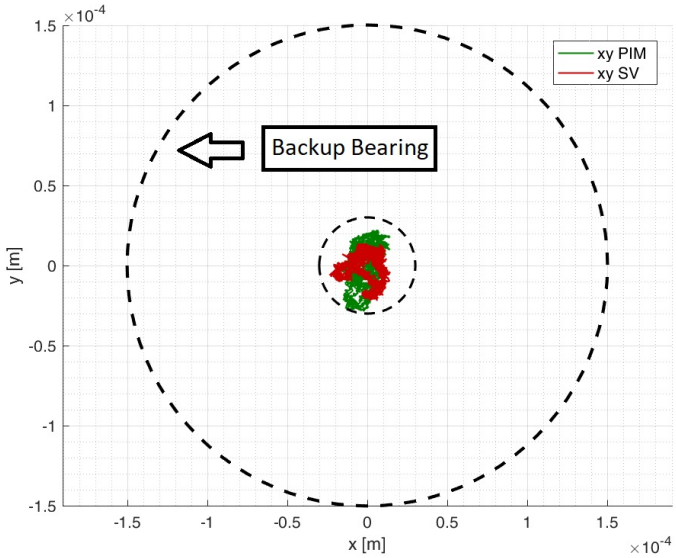

Fig. 10. Trajectory of the rotor with a radial position closed loop control and a partial levitating rotor (one missing bearing) at 3000 rpm speed.

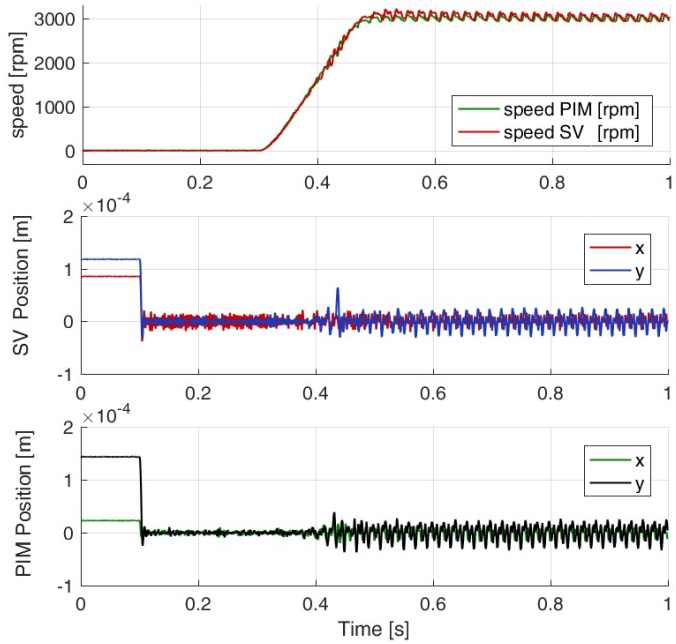

Fig. 11. Radial position of the shaft with a partial levitating rotor (one missing bearing), the position control is activated at 0.1 s and the speed is increased from 0 to 3000 rpm (from 0.3 s to 0.5 s). The two control techniques are compared.

2) Bearingless operation at rated speed: The performance of the position control at 3000 rpm (rated speed) is shown in Fig. 10. The outer circumference shown in the figure represents the backup bearing maximum tolerable displacement ($d_{max} = 150\ \mu m$). It is straightforward to notice that both the control techniques keep the rotor stably centred with a maximum displacement smaller that 30 μm, which is less than 20% of the backup bearing clearance.

3) Acceleration tests for bearingless operation: The position control with a speed transient is shown in Fig. 11, where both the PIM and SV controls allow achieving and maintaining the reference position of the rotor in a similar way. It can be noticed that the initial rotor position is different in the two tests. This is due to the big attraction force between rotor and stator generated by the PMs that tends to push the rotor in the displacement direction as soon as the radial position control is disabled. The above mentioned attraction force can be described by the magnetic stiffness term introduced in [23]. The radial position control is activated at 0.1 s for both the control techniques. It is possible to observe that the SV control is slightly more noisy at stand still than the PIM method and it presents an overshoot during the speed ramp.

VI. Conclusions

TABLE II
Qualitative Comparison

	PIM	SV
Machine efficiency	+	+
Simplicity of the model	+	-
Accuracy of the model	+	-
Performance of the current PI regulators	-	+
Position control performance	+	+

This work aims to compare and experimentally validate two different radial force and torque control methods: the first based on the Moore-Penrose pseudo inverse matrix while the second on the space vector technique. The theoretical aspects of both techniques were already detailed in [22], [23] and [18], [19]. A brief theoretical description is provided in the first part of the manuscript and numerical and FE simulations are used to compare the control techniques.

Table II presents a qualitative comparison of the control methods. It results that the PIM method enables a quick and simple model development and already produces optimized $\alpha - \beta$ axes reference currents in terms of Joule losses minimization. On the other hand, the SV method needs to define a further parameter, $F2_{pu}$, in order to calculate suitable reference current space vectors. The value of $F2_{pu}$ is a degree of freedom that significantly affects the efficiency of the radial force production and in this paper its optimum has been computed through analytical and FE calculations. Furthermore, the contribution of the tangential component of the flux density to the force production is neglected in the SV model in order to simplify its analytical expression. As a consequence, the force coefficients K_{F2} and K_{F4} have to be calculated with FE simulations. On the other hand, both radial and tangential components of the flux density are considered to write the model of the PIM method. Despite the above mentioned disadvantages, the current PI regulators of the SV method work with constant reference current vectors when a rotating force is commanded.

The effectiveness of the PIM and SV methods has been verified by experimental tests for a prototype bearingless MSPM motor where two-DOF ($x - y$ axis position) are successfully controlled. The obtained experimental results validate the models prediction, showing that a stable rotor two-DOF levitation can be achieved by both methods with very similar performance.

TABLE III
JOULE LOSSES PARAMETERS

Parameter	Value
Torque Joule constant (J_T)	24.25 [W/Nm^2]
Force Joule constant 0 ($J_{F,0}$)	0.0148 [W/N^2]
Force Joule constant 1 ($J_{F,1}$)	-0.0319 [W/N^2]
Force Joule constant 2 ($J_{F,2}$)	0.0675 [W/N^2]

APPENDIX

1) Joule Losses - Analytical Evaluation: The stator Joule losses related to a triple three-phase machine are:

$$P_J = \frac{3}{2}R_{ph}(i_{A,d}^2 + i_{A,q}^2 + i_{B,d}^2 + i_{B,q}^2 + i_{C,d}^2 + i_{C,q}^2) \quad (17)$$

written in the d-q rotor reference frame.By means of (12) and (13) it results that the copper Joule losses equation as a function of the $F2_{pu}$ constant and of the reference torque and force is:

$$P_J = \frac{9}{4}R_{ph}(K_{F,d}^2 + K_{F,q}^2)F^2 + \frac{9}{2}R_{ph}(\frac{T}{K_T})^2 \quad (18)$$

with the following set of machine variable (depending by $F2_{pu}$) and constants:

$$\begin{aligned}
K_{F,d} &= C_{m2n4}^{-}\frac{F2_{pu}}{K_{F2}} + C_{m2n2}^{-}\frac{1-F2_{pu}}{K_{F4}} \\
K_{F,q} &= -C_{m2n4}^{+}\frac{F2_{pu}}{K_{F2}} + C_{m2n2}^{+}\frac{1-F2_{pu}}{K_{F4}} \\
C_{m2n4}^{-} &= 3\frac{cm2 - cn4}{cm2^2 - cn2cn4} \\
C_{m2n4}^{+} &= 3\frac{cm2 + cn4}{cm2^2 - cn2cn4} \\
C_{m2n2}^{-} &= 3\frac{cm2 - cn2}{cm2^2 - cn2cn4} \\
C_{m2n2}^{+} &= 3\frac{cm2 + cn2}{cm2^2 - cn2cn4} \\
cm2 &= 1 - 2cos(8\pi/9) \\
cn2 &= 1 - 2cos(4\pi/9) \\
cn4 &= 1 - 2cos(2\pi/9)
\end{aligned} \quad (19)$$

In (18) $F2_{pu}$ is explicit and its optimised value is easily found as:

$$\frac{dP_J}{dF2_{pu}} = 0 \quad (20)$$

resulting in:

$$F2_{pu} = -\frac{J_{F,1}}{2J_{F,2}} = 0.236 \quad (21)$$

The analytical optimised $F2_{pu}$ value is in good agreement with the one obtained with FEA.

REFERENCES

[1] T. Baumgartner, R. M. Burkart, and J. W. Kolar, "Analysis and design of a 300-w 500000-r/min slotless self-bearing permanent-magnet motor," *IEEE Transactions on Industrial Electronics*, vol. 61, no. 8, pp. 4326–4336, Aug 2014.

[2] A. Chiba, T. Fukao, O. Ichikawa, M. Oshima, M. Takemoto, and D. G. Dorrell, *Magnetic bearings and bearingless drives*. Elsevier, 2005.

[3] A. H. Pesch, A. Smirnov, O. Pyrhnen, and J. T. Sawicki, "Magnetic bearing spindle tool tracking through μ -synthesis robust control," *IEEE/ASME Transactions on Mechatronics*, vol. 20, no. 3, pp. 1448–1457, June 2015.

[4] S. Y. Zhang, C. B. Wei, J. Li, and J. H. Wu, "Robust h controller based on multi-objective genetic algorithms for active magnetic bearing applied to cryogenic centrifugal compressor," in *2017 29th Chinese Control And Decision Conference (CCDC)*, May 2017, pp. 46–51.

[5] C. Peng, J. Sun, X. Song, and J. Fang, "Frequency-varying current harmonics for active magnetic bearing via multiple resonant controllers," *IEEE Transactions on Industrial Electronics*, vol. 64, no. 1, pp. 517–526, Jan 2017.

[6] A. Chiba, M. A. Rahman, and T. Fukao, "Radial force in a bearingless reluctance motor," *IEEE Transactions on Magnetics*, vol. 27, no. 2, pp. 786–790, March 1991.

[7] T. Schneider and A. Binder, "Design and evaluation of a 60 000 rpm permanent magnet bearingless high speed motor," in *2007 7th International Conference on Power Electronics and Drive Systems*, Nov 2007, pp. 1–8.

[8] X. Sun, Z. Xue, J. Zhu, Y. Guo, Z. Yang, L. Chen, and J. Chen, "Suspension force modeling for a bearingless permanent magnet synchronous motor using maxwell stress tensor method," *IEEE Transactions on Applied Superconductivity*, vol. 26, no. 7, pp. 1–5, Oct 2016.

[9] S. Serri, A. Tani, and G. Serra, "A method for non-linear analysis and calculation of torque and radial forces in permanent magnet multiphase bearingless motors," in *International Symposium on Power Electronics Power Electronics, Electrical Drives, Automation and Motion*, June 2012, pp. 75–82.

[10] J. Huang, B. Li, H. Jiang, and M. Kang, "Analysis and control of multiphase permanent-magnet bearingless motor with a single set of half-coiled winding," *IEEE Transactions on Industrial Electronics*, vol. 61, no. 7, pp. 3137–3145, July 2014.

[11] B. Li, J. Huang, H. Liu, and Z. Hou, "Analysis and control of seven-phase permanent-magnet bearingless motor with single set of half-coiled winding," in *2014 IEEE 23rd International Symposium on Industrial Electronics (ISIE)*, June 2014, pp. 2080–2086.

[12] X. L. Wang, Q. C. Zhong, Z. Q. Deng, and S. Z. Yue, "Current-controlled multiphase slice permanent magnetic bearingless motors with open-circuited phases: Fault-tolerant controllability and its verification," *IEEE Transactions on Industrial Electronics*, vol. 59, no. 5, pp. 2059–2072, May 2012.

[13] M. Ramezani and O. Ojo, "The modeling and position-sensorless estimation technique for a nine-phase interior permanent-magnet machine using high-frequency injections," *IEEE Transactions on Industry Applications*, vol. 52, no. 2, pp. 1555–1565, March 2016.

[14] A. Tani, Y. Gritli, M. Mengoni, L. Zarri, G. Sala, A. Bellini, and G. Serra, "Detection of magnet demagnetization and high-resistance connections in five-phase surface-mounted permanent magnet generators," in *2015 IEEE 10th International Symposium on Diagnostics for Electrical Machines, Power Electronics and Drives (SDEMPED)*, Sept 2015, pp. 487–493.

[15] M. Mengoni, L. Zarri, A. Tani, Y. Gritli, G. Serra, F. Filippetti, and D. Casadei, "Online detection of high-resistance connections in multiphase induction machines," *IEEE Transactions on Power Electronics*, vol. 30, no. 8, pp. 4505–4513, Aug 2015.

[16] A. Tani, M. Mengoni, L. Zarri, G. Serra, and D. Casadei, "Control of multiphase induction motors with an odd number of phases under open-circuit phase faults," *IEEE Transactions on Power Electronics*, vol. 27, no. 2, pp. 565–577, Feb 2012.

[17] H. S. Che, M. J. Duran, E. Levi, M. Jones, W. P. Hew, and N. A. Rahim, "Postfault operation of an asymmetrical six-phase induction machine with single and two isolated neutral points," *IEEE Transactions on Power Electronics*, vol. 29, no. 10, pp. 5406–5416, Oct 2014.

[18] G. Sala, D. Gerada, C. Gerada, and A. Tani, "Radial force control for triple three-phase sectored spm machines. part i: Machine model," in *2017 IEEE Workshop on Electrical Machines Design, Control and Diagnosis (WEMDCD)*, April 2017, pp. 193–198.

[19] ——, "Radial force control for triple three-phase sectored spm machines. part ii: Open winding fault tolerant control," in *2017 IEEE Workshop on Electrical Machines Design, Control and Diagnosis (WEMDCD)*, April 2017, pp. 275–280.

[20] M. Barcaro, N. Bianchi, and F. Magnussen, "Faulty operations of a pm fractional-slot machine with a dual three-phase winding," *IEEE Transactions on Industrial Electronics*, vol. 58, no. 9, pp. 3825–3832, Sept 2011.

[21] L. Alberti and N. Bianchi, "Impact of winding arrangement in dual 3-phase induction motor for fault tolerant applications," in *The XIX International Conference on Electrical Machines - ICEM 2010*, Sept 2010, pp. 1–6.

[22] G. Valente, L. Papini, A. Formentini, C. Gerada, and P. Zanchetta, "Radial force control of multi-sector permanent magnet machines," in

2016 XXII International Conference on Electrical Machines (ICEM), Sept 2016, pp. 2595–2601.

[23] ——, "Radial force control of multi-sector permanent magnet machines considering radial rotor displacement," in *2017 IEEE Workshop on Electrical Machines Design, Control and Diagnosis (WEMDCD)*, April 2017, pp. 140–145.

[24] S. Zhou and J. Shi, "Active balancing and vibration control of rotating machinery: a survey," *Shock and Vibration Digest*, vol. 33, no. 5, pp. 361–371, 2001.

[25] A. Galassini, G. L. Calzo, A. Formentini, C. Gerada, P. Zanchetta, and A. Costabeber, "ucube: Control platform for power electronics," in *2017 IEEE Workshop on Electrical Machines Design, Control and Diagnosis (WEMDCD)*, April 2017, pp. 216–221.

G. Sala was born in Vercelli, Italy, in 1990. He received the B. Sc. in Power Engineering in 2012 and the M. Sc. degree in Electrical Engineering, with honors, in 2014 from the University of Bologna, Bologna, Italy. Since 2014 he has been working toward the Ph.D. degree at the Department of Electrical, Electronic and Information Engineering, University of Bologna. He is currently a research associate of the Power Electronics, Machines and Control Group, Department of Electrical and Electronic Engineering, Faculty of Engineering, The University of Nottingham, Nottingham. His research interests include modelling and control of multiphase machines, fault tolerant control and fault diagnosis of electrical drives.

G. Valente received his Bachelor degree in Energy Engineering in 2011 and his Master degree in Electrical Engineering in 2014 both from the University of Padova, Italy. Between 2013 and 2014 he developed sensorless control techniques for PMSM for his Master thesis at the University of Oviedo, Spain. He is now working towards its Ph.D. with the Power Electronics, Machines and Control Group, University of Nottingham, UK. His main research interest is design and control of electrical machines.

A. Formentini received the M.S. degree in computer engineering and the PhD degree in electrical engineering from the University of Genova, in 2010 and 2014 respectively. Since 2014 he is research fellow in the Power Electronics, Machines and Control Group, University of Nottingham, UK. His research interests include control systems applied to electrical machine drives and power converters.

L. Papini received his Bachelor degree (Hons.) and Master degree (Hons.) in Electrical engineering in 2009 and 2011, respectively, both from the University of Pisa, Italy. He's been a visiting student at The University of Nottingham, UK, developing analytical and numerical models for electrical machines. From June to November 2011 he collaborated with the Department of Energy Engineering, University of Pisa, as a research assistant. He is currently working towards its Ph.D. with the Power Electronic, Motors and Drives Group at University of Nottingham. Since 2013 hold a position of research assistant in the same institution. His main research interests are high speed, high power density electric machines, machine control and levitating system.

D. Gerada received the B.Eng.(Hons.) degree in electrical engineering from the University of Malta, Malta in 2007 and the Ph.D. degree in high-speed electrical machines from the University of Nottingham, Nottingham, UK in 2012. From 2007-2016 he was with the R&D Department at Cummins Generator Technologies, Stamford, UK, first as an Electrical Machine Design Engineer (2007-2011) and then as a Senior Electrical Machine Design Engineer and Innovation Leader (2011-2016). In 2016 he joined the University of Nottingham as a Senior Research Fellow in Electrical Machines. His research interests include high speed machines, traction machines, use of novel materials, and multiphysics-based optimization of electrical machines. Dr. Gerada is a Chartered Engineer in the U.K. and a member of the Institution of Engineering and Technology.

P. Zanchetta (M 00, SM 15) received his MEng degree in Electronic Engineering and his Ph.D. in Electrical Engineering from the Technical University of Bari (Italy) in 1993 and 1997 respectively. In 1998 he became Assistant Professor of Power Electronics at the same University. In 2001 he became lecturer in control of power electronics systems in the PEMC research group at the University of Nottingham UK, where he is now Professor in Control of Power Electronics systems. He has published over 270 peer reviewed papers and he is Senior Member of the IEEE. He is Chair of the IAS Industrial Power Converter Committee IPCC and member of the European Power Electronics (EPE) executive board. His research interests include control of power converters and drives, Matrix and multilevel converters, power electronics for energy and transportation.

A. Tani was born in Faenza, Italy, in 1963. He received the M. Sc. in Electrical Engineering, with honors, from the University of Bologna, Bologna, Italy, in 1988. Currently he is a Full Professor of power electronics, electrical machines and drives with the Department of Electric, Electronic and Information Engineering, University of Bologna. He has authored more than 170 papers published in technical journals and Conf. proceedings. His current activities include multiphase motor drives, ac/ac matrix converters, and field weakening strategies for induction motor drives.

C. Gerada (M 05) received the Ph.D. degree in numerical modelling of electrical machines from The University of Nottingham, Nottingham, U.K., in 2005. He subsequently worked as a Researcher with The University of Nottingham on high-performance electrical drives and on the design and modelling of electromagnetic actuators for aerospace applications. Since 2006, he has been the Project Manager of the GE Aviation Strategic Partnership. In 2008, he was appointed as a Lecturer in electrical machines; in 2011, as an Associate Professor; and in 2013, as a Professor at The University of Nottingham. His main research interests include the design and modelling of high-performance electric drives and machines. Prof. Gerada serves as an Associate Editor for the IEEE TRANSACTIONS ON INDUSTRY APPLICATIONS and is the past Chair of the IEEE IES Electrical Machines Committee.